Superpixel based sea ice segmentation with high-resolution optical images: analysis and evaluation.

CHEN, S., YAN, Y., REN, J., HWANG, B., MARSHALL, S. and DARRANI, T.

2022

Superpixel Based Sea Ice Segmentation with High-Resolution Optical Images: Analysis and Evaluation

Siyuan Chen[1], Yijun Yan[2], Jinchang Ren[2*], Phil Hwang[3], Stephen Marshall[1], Tariq Durrani[1]

Abstract. By grouping pixels with visual coherence, superpixel algorithms provide an alternative representation of regular pixel grid for precise and efficient image segmentation. In this paper, a multi-stage model is used for sea ice segmentation from the high-resolution optical imagery, including the pre-processing to enhance the image contrast and suppress the noise, superpixel generation and classification, and post-processing to refine the segmented results. Four superpixel algorithms are evaluated within the framework, i.e. SLIC, BASS, TS-SLIC and WP, where the high-resolution imagery of the Chukchi sea is used for validation. Overall, the model yields a segmentation accuracy of 98.19% on average and adhere the ice edges well. We also present quantitative evaluation in terms of the segmentation quality and floe size distribution, and visual comparison with several selected regions of interest. It is found that TS-SLIC performs the best within the group.

Keywords: sea ice segmentation; superpixel; satellite remote sensing.

1 Introduction

With the trend of global warming, the global climate changes in the last few decades significantly affect the Arctic Ocean area [1], leading to the decline of the Arctic sea ice extent. According to the Arctic amplification phenomenon, the trends of temperature variation are more obvious in the Arctic region than that of the northern hemisphere or the globe as a whole [2]. To understand the ongoing sea ice changes, it is valuable to investigate the dimension of the marginal ice zone (MIZ). MIZ is defined as the transitional region between the open sea and dense drift ice, and it is closely correlated to the representation of sea ice in the climate and weather models [3]. Nevertheless, MIZ is vulnerable to open ocean processes such as waves and wind [4], which makes its size unpredictable and hard to be detected correctly.

High-resolution optical (HRO) imagery, the satellite image with a relative high spatial resolution, offers the potential for precisely identifying the location of the boundary between sea ice and open water, i.e. so called ice edges [5], and accurately determining the floe size distribution (FSD). Recent years, as the HRO images have become more accessible, various approaches have been developed for sea ice segmentation, including

J. Ren (✉), National Subsea Centre, Robert Gordon University, Aberdeen, U.K., e-mail: j.ren@rgu.ac.uk. This work was supported in part by the Natural and Environmental Research Council under the Grant NE/S002545/1, U.K.

the combination of the maximum cross-correlation techniques and multi-sensor HRO images [6], the combination of the watershed transformation and random forest classification [7], and the texture-sensitive superpixel based segmentation [8]. To tackle the high computation complexity of the HRO imagery, superpixel algorithms provide an alternative representation of regular pixel grid by grouping the similar pixels into over-segmented small regions. The generated superpixels can accordingly reduce the complexity for subsequent processing whilst adhering well to the boundaries of ice floes and open water. For instance, the simple linear iterative clustering (SLIC) superpixel is combined with the minimum spanning tree in [9], and the random forest is used for grouping the superpixels produced by the SLIC algorithm in [10].

Motivated by the aforementioned challenges and inspired by some existing works, this paper therefore, aims at evaluating the performance of different superpixel algorithms for sea ice segmentation from HRO imagery within a multi-stage model framework, which includes contrast enhancement and noise removal, superpixel generation and grouping, followed by a morphological opening process as post-processing. To evaluate the model, the selection of the superpixel number is investigated. The proposed modal is also compared against two state-of-the-art image segmentation methods quantitatively and qualitatively.

2 Superpixel Based Sea Ice Segmentation

2.1 The Framework

The framework of the multi-stage model is presented in Fig. 1, which includes three main stages. Firstly, the image is pre-processed via the Top-Hat and Bottom-Hat transforms, the widely used detail enhancing approach in medical image processing [11], which allows the segmentation of the small ice floes from the ice-water mixed regions with low contrast. The bilateral filter [12] is then employed for noise removal whilst preserving the edge information. By adding the Top-Hat and subtracting the Bottom-Hat on the original image, the processed image shows enhanced foreground and suppressed background, which is beneficial for the following-on segmentation process.

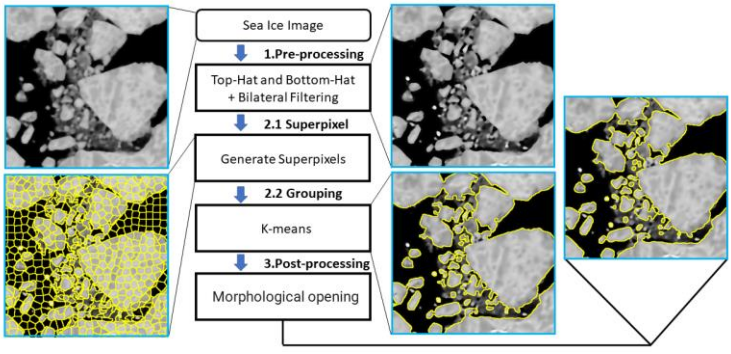

Fig. 1 Workflow of the multi-stage segmentation model

Next, superpixel segmentation is generated. In this study, we have employed four algorithms for comparison, including the SLIC [13], Texture Sensitive SLIC (TS-SLIC) [8], Water Pixel (WP) [14], and Bayesian Adaptive Superpixel Segmentation (BASS) [15]. Next, k-means is applied to split the superpixels into two classes, namely water and ice, based on the mean intensity and standard deviation of each individual superpixel. Then the classified superpixels are merged to form the segmented result. Finally, the segmented result is refined by morphological opening as post-processed to smooth the ice shapes and also separate the connected floes. Regarding the morphological operations, depending on the size of structuring element (SE), the result may vary a lot. In this study, disk shape SE was chosen as most objects of interest have arcuate boundaries, where the radius is set to $R = 5$ in the pre-processing stage for better noise removal whilst preserving enough texture information, and $R = 3$ in the post-processing stage for refining the segmented result whilst retaining the small floes.

2.2 Superpixel Algorithms and Implementation

As one of the most popular superpixel algorithms, SLIC groups the pixels with the local k-means clustering that searches the pixels in a limited region centered at each cluster center based on the distance, D, that considering both the colour and spatial Euclidean distances, namely d_c and d_s, as defined below:

$$d_c = \sqrt{(l_j - l_i)^2 + (a_j - a_i)^2 + (b_j - b_i)^2} \tag{2.1}$$

$$d_s = \sqrt{(x_j - x_i)^2 + (y_j - y_i)^2} \tag{2.2}$$

where the vector (l, a, b) denotes the values of three colour components in the CIELAB colour space, and (x, y) is the spatial coordinate of each pixel. Let N be the total number of pixels in the input image, and K is the superpixel number, the sampling interval, S, accordingly can be derived, $S = \sqrt{N/K}$ [13]. By further introducing the compactness coefficient, m, the final distance can be determined as:

$$D = \sqrt{(d_c)^2 + (\frac{d_s}{S} m)^2} \tag{2.3}$$

The distance in TS-SLIC contains a texture descriptor d_t, and a local directional zigzag pattern (LDZP [16]). As a result, the generated superpixel become more sensitive to the texture information, where the d_t is given by:

$$d_t = \sqrt{\sum_{n=1}^{N_r} (LDZP_{i,n} - LDZP_{j,n})^2} \tag{2.4}$$

where N_r is the number of neighbouring pixels in a selected local window (i.e. $N_r = 8$ for a 3 by 3 window).

Similarly, the compactness refined distance, D', can be derived as:

$$D' = \sqrt{(d_c)^2 + (\frac{d_s}{S})^2 m^2 + d_t} \quad (2.5)$$

The Water Pixel algorithm first converts the original image to a gradient image and generates the initial seeds. This is achieved by defining a regular hexagonal grid according to the predefined grid step, σ, then investigating the regions with minimum gradient values inside the individual cells. Next, the image is distance transformed based on the seed regions and added to the gradient image with multiplying a regularisation parameter, k_{wp}, enforcing the compactness of the latter superpixels generation. Consequently, the superpixels are determined by performing the watershed transforms on the regularised gradient image.

The BASS algorithm is a refinement of the Direchlet-Process Gaussian Mixture Model (DPGMM), which is a Bayesian Non-Parametric (BNP) mixture model. By introducing the Potts term to the Bayesian estimation of the spatial covariances, the resulting superpixels respect more spatial coherence than the DPGMM. Moreover, BASS can produce size-adaptive superpixels without predefining the superpixel number by iteratively evaluating the split and merged supeprixel proposals through the Hastings ratios, encouraging the superpixels to retain only the connected regions.

For implementation, the parameters need to be specified. In this study, we adopted the compactness coefficient $m = 10$ for both SLIC and TS-SLIC, and the regularisation parameter k_{wp} is set to 8 for WP. The gradient image used for WP is produced by performing a basic morphological gradient using the SE with the radius $R = 3$. Additionally, since BASS does not allow manual parameter setting, we directly take the published results for comparison. Regarding the superpixel number, we analyse its effect on the segmentation results in Section 3.3.

3 Experiments and Discussions

3.1 Source Data and Ground Truth (GT)

The studied area is centered at around $69^{\circ}56'N/170^{\circ}00'W$ in the Chukchi Sea. The source data [17] is provided by the U.S. Geological Survey (USGS), which is available in the Global Fiducials Library, a long-term archive of the images from U.S. National Imagery Systems. The image is in grayscale where the acquired date was 31 May 2013. In this study, the GT data is generated via the methodology proposed in study [18], where the interested region was firstly cropped out and downsized, then the environment for visualizing images (ENVI) software was used to produce automated segmentation result, followed by manual correction by domain experts. In addition, since the algorithms (i.e. SLIC), require RGB imagery as the input, the grayscale HRO image is duplicated into the three colour bands for meeting the need.

3.2 Evaluation Metrics

To subjectively evaluate the segmentation results, several popularly used metrics are selected, including pixel accuracy (ACC), Matthews correlation coefficient (MCC),

and conformity coefficient (CC) [19-21]. In addition, to evaluate the FSD, the segmented floes with 8 connectivity are quantified into nine categories according to the size ranged in $[10^{i-1}, 10^{i}]$ pixels, where $i = [1,9]$. The occurrence frequencies of the floes in nine categories can be seen as a vector. Then, the person correlation coefficient (PCC) is used for measuring the linear correlation between vectors A and B, the vectors of normalised floe occurrence frequencies from the GT and the segmented results, respectively. The definitions of these metrics are summarised as follows:

$$ACC = (TP + TN)/(TP + TN + FP + FN) \tag{3.1}$$

$$MCC = \frac{TP \cdot TN - FP \cdot FN}{\sqrt{(TP+FP)\cdot(TP+FN)\cdot(TN+FP)\cdot(TN+FN)}} \tag{3.2}$$

$$CC = 1 - (FP + FN)/TP \tag{3.3}$$

$$PCC(A,B) = \frac{\sum(A_i-\bar{A})(B_i-\bar{B})}{\sqrt{\sum(A_i-\bar{A})^2 \sum(B_i-\bar{B})^2}}, where\ i = [1,9] \tag{3.4}$$

where TP, TN, FP, FN are respectively the pixel level true positive, true negative, false positive, and false negative from the confusion matrix. $\bar{A}$ and $\bar{B}$ are the mean values of vectors A and B.

3.3 Evaluation of the number of superpixels

To evaluate the effect of different numbers of superpixels to the three superpixel number adjustable algorithms, we change the K from 1×10^4 to 10×10^4 with an increment of 1×10^4 for SLIC and TS-SLIC algorithms, and adjust the grid step, σ, in the WP algorithm to change the superpixel number with an increment of around 1×10^4. Worth noting that WP only support uint16 format as the output, resulting in the superpixel number being limited. The results are presented in Fig. 2.

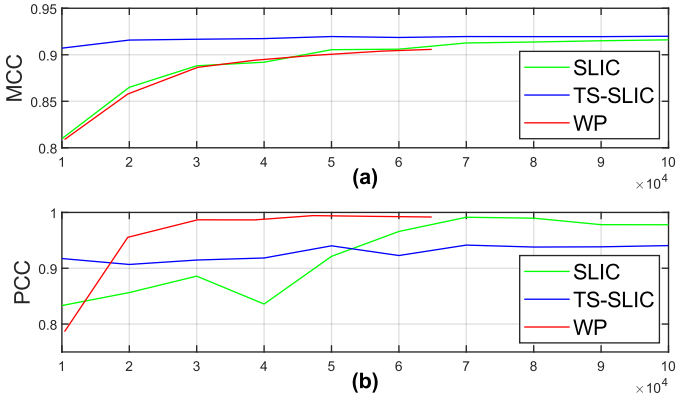

Fig. 2 (a) MCC and (b) PCC scores versus the superpixel number

As seen in Fig. 2(a) and (b), the TS-SLIC algorithm shows a better invariance against the superpixel number variation than the others in both segmentation quality and FSD, and the algorithm can be seen achieves higher MCC when superpixel number is low. The MCC scores of SLIC and WP by contrast firstly increase rapidly as the superpixel number increases and become stable after certain values. The PCC scores of WP similarly firstly shows a growing trend and maintains a high level. The highest PCC scores are achieved when the superpixel number is $K = 7 \times 10^4$ for both SLIC and TS-SLIC, and $\sigma = 20$ (corresponding $K = 47212$) for WP. Hence, in the following experiments, we adopt $K = 7 \times 10^4$ for SLIC and TS-SLIC, and $\sigma = 20$ for WP for simplicity.

3.4 Results and Analysis

Fig. 3 presents the visual comparison of three cropped regions of interest (ROIs). In the green bounding box, the floes are concentrated with poor boundary, where SLIC and TS-SLIC outperform the other two approaches in terms of relatively successfully separated connected floes whilst adhering well the boundary. In the low contrast water-ice mixed region, as highlighted in the blue bounding box, TS-SLIC shows a superior performance in identifying these small floes. However, as seen in the yellow bounding-box, BASS has a better performance in adhering the boundaries of melt ponds inside the floes even than the GT.

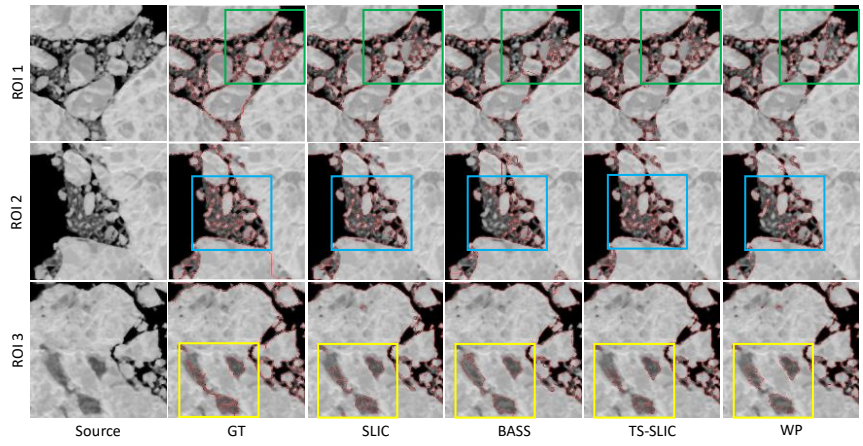

Fig. 3 ROI visual comparison

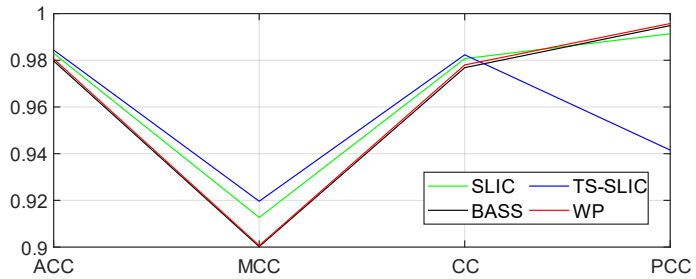

Fig. 4 Quantitative results of four superpixel algorithms

Fig. 4 shows the detailed performance of the model when integrating different algorithms. Although all algorithms have yielded overall good performance, the TS-SLIC can be seen to slightly outperform the competitors in terms of the accuracy, MCC and CC, which is therefore the best method in terms of segmentation quality. However, it is somewhat surprising that TS-SLIC has the lowest floe size distribution similarity to the ground truth. To investigate the reason, the relative distribution histogram is derived and shown in Fig. 5, where TS-SLIC tends to extract more small floes within the size ranging from 10 to 100 pixels than the other three algorithms. This can also be obtained directly from the blue bounding box in Fig. 3. This, however, may not be accounted as the drawback of this algorithm as extracting small floes are extremely valuable for FSD.

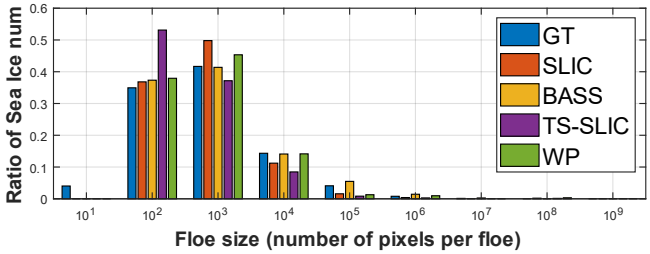

Fig. 5 Histogram comparison of the FSDs.

To further evaluate the segmentation quality and model efficiency, the segmentation result is compared with the Open Source Sea-ice Processing (OSSP) method [7] and the algorithm [22] based on the hidden Markov random field (HMRF) model and its expectation-maximization (EM) with the iteration number set to 10. All the experiments were executed on a computer with 4.1 GHz CPU and 16 GB RAM. The results are given in Table 1, where the SLIC result slightly outperforms the others, which validates the efficacy of the model. Our model, however, takes around 46 seconds longer than OSSP, in which the bilateral filtering takes around 42 seconds. The efficiency thus needs to be further improved in the future work. Additionally, the running time will be extended when using the BASS algorithm to generate superpixels due to the algorithm complexity, which is considered as a drawback in the HRO image processing.

Table 1 Quantitative comparison to other segmentation methods using the SLIC result.

Method	Platform	ACC	MCC	CC	PCC	Time (s)
OSSP	Python	98.26	90.94	98.04	98.45	41
HMRF-EM	MATLAB	93.47	76.26	92.07	95.22	359
Our model	MATLAB	98.30	91.27	98.07	99.14	87

4. Conclusions

This paper presents the sea ice segmentation from HRO imagery using a superpixel based multi-stage model, where the effect of the superpixel number and the performance of four superpixel algorithms are evaluated. Consequently, the algorithms showed an overall good performance, among which the TS-SLIC outperforms three others slightly in terms of the segmentation quality and extraction of small floes. The BASS performs the best in adhering the boundary of the melting ponds, however, it is computationally extensive has limited its application in HRO imagery processing. In

the future work, we plan to apply the superpixel based method to the HRO images even with a low contrast and complex environmental issues (i.e. cloudy), which are the main issues that the optical images usually have. To accurately investigate ice regions in such images, the superpixel, as a compact intermediate image representation, can be combined with the supervised models such as the deep learning methods to further improve the performance whilst speeding up the computation.

References

1. Stroeve, J., et al., *Arctic sea ice decline: Faster than forecast.* Geophysical Research Letters, 2007. **34**(9): p. n/a-n/a.
2. Serreze, M.C. and R.G. Barry, *Processes and impacts of Arctic amplification: A research synthesis.* Global and planetary change, 2011. **77**(1-2): p. 85-96.
3. Batrak, Y. and M. Müller, *Atmospheric Response to Kilometer-Scale Changes in Sea Ice Concentration Within the Marginal Ice Zone.* Geophysical Research Letters, 2018. **45**(13): p. 6702-6709.
4. Meylan, M.H., et al., *Dispersion Relations, Power Laws, and Energy Loss for Waves in the Marginal Ice Zone.* Journal of Geophysical Research: Oceans, 2018. **123**(5): p. 3322-3335.
5. Scheuchl, B., et al., *Potential of RADARSAT-2 data for operational sea ice monitoring.* Canadian Journal of Remote Sensing, 2004. **30**(3): p. 448-461.
6. Kim, C.-U.H.a.H.-c., *A Feasibility Study of Sea Ice Motion and Deformation Measurements Using Multi-Sensor High-Resolution Optical Satellite Images.* Remote Sensing, 2017. **9**(9): p. 930.
7. Wright, N.C. and C.M. Polashenski, *Open-source algorithm for detecting sea ice surface features in high-resolution optical imagery.* The Cryosphere, 2018. **12**(4): p. 1307-1329.
8. Chai, Y., et al., *Texture-Sensitive Superpixeling and Adaptive Thresholding for Effective Segmentation of Sea Ice Floes in High-Resolution Optical Images.* IEEE Journal of Selected Topics in Applied Earth Observations and Remote Sensing, 2021. **14**: p. 577-586.
9. Wang, M., et al., *Optimal Segmentation of High-Resolution Remote Sensing Image by Combining Superpixels With the Minimum Spanning Tree.* IEEE Transactions on Geoscience and Remote Sensing, 2018. **56**(1): p. 228-238.
10. Csillik, O., *Fast Segmentation and Classification of Very High Resolution Remote Sensing Data Using SLIC Superpixels.* Remote Sensing, 2017. **9**(3): p. 243.
11. Kushol, R., et al., *Contrast Enhancement by Top-Hat and Bottom-Hat Transform with Optimal Structuring Element: Application to Retinal Vessel Segmentation*. 2017, Springer International Publishing. p. 533-540.
12. Tomasi, C. and R. Manduchi. *Bilateral filtering for gray and color images*. in *Sixth international conference on computer vision (IEEE Cat. No. 98CH36271)*. 1998. IEEE.
13. Achanta, R., et al., *SLIC superpixels compared to state-of-the-art superpixel methods.* IEEE transactions on pattern analysis and machine intelligence, 2012. **34**(11): p. 2274-2282.
14. Machairas, V., et al., *Waterpixels.* IEEE Transactions on Image Processing, 2015. **24**(11): p. 3707-3716.
15. Uziel, R., M. Ronen, and O. Freifeld. *Bayesian adaptive superpixel segmentation*. in *Proceedings of the IEEE/CVF International Conference on Computer Vision*. 2019.
16. Roy, S.K., et al., *Local directional ZigZag pattern: A rotation invariant descriptor for texture classification.* Pattern Recognition Letters, 2018. **108**: p. 23-30.
17. U.S. Geological Survey, *Chukchi_20130531_2*. 2013; Available from: https://lta.cr.usgs.gov/gfl/index.php?img:3858:124&PTAGNAME=ArcticSea.
18. Hwang, B., et al., *A practical algorithm for the retrieval of floe size distribution of Arctic sea ice from high-resolution satellite Synthetic Aperture Radar imagery.* Elementa: Science of the Anthropocene, 2017. **5**.
19. Chang, H.-H., et al., *Performance measure characterization for evaluating neuroimage segmentation algorithms.* NeuroImage, 2009. **47**(1): p. 122-135.
20. Chicco, D. and G. Jurman, *The advantages of the Matthews correlation coefficient (MCC) over F1 score and accuracy in binary classification evaluation.* BMC Genomics, 2020. **21**(1).
21. Taha, A.A. and A. Hanbury, *Metrics for evaluating 3D medical image segmentation: analysis, selection, and tool.* BMC Medical Imaging, 2015. **15**(1).
22. Wang, Q., *HMRF-EM-image: Implementation of the Hidden Markov Random Field Model and its Expectation-Maximization Algorithm.* arXiv pre-print server, 2012.